Sensors and Materials, Vol. 18, No. 4 (2006) 215–229
MYU Tokyo

S & M 0644

Detecting Embedded Objects Using Haptics with Applications in Artificial Palpation of Tumors

Siamak Najarian, Javad Dargahi[1,*] and Vahid Mirjalili[2]

Biomedical Engineering, Biomechanics Department, Faculty of Biomedical Engineering,
Amirkabir University of Technology, Hafez Avenue, Tehran, Iran
[1]Department of Mechanical and Industrial Engineering, Concordia University,
1455 de Maisonneuve Blvd. West, Montreal, Quebec, Canada H3G 1M8.
[2]CONCAVE Research Centre, CR-200, Concordia University,
Department of Mechanical and Industrial Engineering, 1455 de Maisonneuve Blvd.
West, Montreal, Quebec, Canada
H3G 1M8

(Received August 8, 2005; accepted April 14, 2006)

Key words: breast tumors, tactile sensor, noninvasive examination, mammography

In this paper, we describe a new method of measuring the stiffness of embedded objects. A tailor-made tactile probe equipped with a polyvinylidene fluoride-based (PVDF-based) piezoelectric sensor was used in the experimental tests. The structure of the probe is such that it deforms in specific ways when pressed against a large object. Two elastic materials, in the form of two concentric cylinders, with different moduli of elasticity compose the major structure of the sensor assembly. Young's modulus for a hidden object located inside a block is determined experimentally when the probe is applied to the outside of a rubberlike matrix. This matrix simulates the human organs (such as the breast). We propose a new analytical method that can be employed as a predictive tool for determining the stiffness and certain details of the geometry of embedded objects. In addition to the analytical method, a numerical approach is utilized in parallel, which is based on finite element analysis. The difference between the two theoretical methods is proven to be very small, and for all practical purposes, they can both be considered effective in our research. A reasonably good correspondence between the analytical and numerical approaches is obtained. The findings of this work have practical applications in detecting cancerous tumors in breast examination procedures.

1. Introduction

There are different methods of detecting breast cancer, which is the most common form of cancer in women.[(1)] This disease can be detected either manually, e.g., by clinical breast examination (CBE), or by medical imaging methods such as mammography or ultrasonography. Mammography has been proven to reduce mortality from breast cancer, and in this

*Corresponding author, e-mail address: jdargahi@alcor.concordia.ca

method, X-rays are used to examine a patient's breast. The early stages of breast cancer may not have any symptoms; therefore, it is crucial for women to strictly follow screening recommendations. As it increases in size, a cancerous tumor can cause various changes such as a change in the size or shape of the breast.[2] Another detection procedure is ultrasonography. This is recommended when the physicians suspect the existence of a hard lump or cyst in the breast. In this case, the patient is recommended to undergo ultrasonography, which does not involve the use of X-rays; hence, it is less dangerous than other imaging methods.

In CBE, a clinician palpates the patient to search for any lumps or changes in the breast tissue that could indicate the presence of a tumor. The major advantage of this examination is that it is not invasive and does not require radiation. However, it cannot provide the clinician with much information about the lump. Consequently, if a lump is detected through palpation, typically all that can be documented is its general location in the breast and an approximation of its size. To address this problem, a medical probe equipped with a special tactile sensor was developed, which can be used in place of the physician's fingertips.[3–6] As the probe is pressed against the skin of the patient, a tactile mapping of the tissue can be generated, owing to the contact pressure between the probe and the biological tissue and recorded for further studies.

In this research work, we discuss the application of a probe that could determine the stiffness of embedded objects only on the basis of haptics. That is, by just touching and gently exerting mild pressures on the skin, some useful information on the stiffness and geometry of tumors or objects can be gained. This has immediate applications in breast cancer detection. To accomplish this, first, we developed a mathematical formulation of this phenomenon. A relationship is derived between the displacement on the surface of the skin and the mechanical properties of normal tissue and tumors. Here, we utilized the finding that breast tumors have a higher modulus of elasticity than neighboring normal tissue.[7] Therefore, tissue stiffness is different in different places and this property can be detected by placing a tactile probe on different locations on the skin. Once we manage to detect a difference in the softness of tissue, we will obtain some vital information about embedded tumors.[8] A brief summary of the research activities, including the authors' contribution in this area, is given below.

The medical applications of tactile sensing using a polyvinylidene fluoride (PVDF) film as a transducer have been investigated.[9–14] In a research using a modified commercial endoscopic tool, applied force was measured by strain gauges, and then the position of the grasper was determined with an optical detector.[15] In that study, force displacement data were obtained and objects with five different elastic properties were identified. The compliance of a hard rubber embedded in a block of foam by remote palpation has been reported.[16] Additionally, an endoscopic and robotic micromachined sensor has been designed and fabricated using a PVDF film.[17] The design, fabrication, and theoretical studies of a micromachined piezoelectric tactile sensor for an endoscopic grasper have been carried out.[18] The sensor exhibited a high force sensitivity, a high dynamic range, a good linearity, and a high signal-to-noise ratio. Using a pneumatic propulsion method, a microrobot has been designed for colonoscopic surgeries.[19] A prototype of an endoscopic toothlike piezoelectric tactile sensor has been developed for measuring both the compli-

ance and surface profiles of biological tissues.[20] It consists of a rigid cylinder surrounded by a compliant cylinder. The rigid and compliant cylinders are fabricated from Plexiglas and an elastomer, respectively. Detailed experimental tests and finite element analysis of this proposed sensor have also been attempted.[21] Furthermore, a preliminary micromachined version of the same sensor has successfully been built.[22] In other research, a force moment sensor has been placed into the distal shaft of laparoscopic forceps in addition to a tactile sensor array being placed between the jaws of the forceps.[23] The piezoresistive sensor array used was a foil sensor with 64 measuring points. In another work, the pyroelectric effects associated with PVDF-based tactile sensors were separated from the piezoelectric effect using different methods.[24] This device has provided an alternative transient approach to distinguishing between piezoelectric and pyroelectric signals using only one single PVDF layer film, thereby, reducing the complexity of the sensor.

2. Materials and Methods

2.1 *Sensor design*

Figure 1 shows a computer-generated model of the sensor (i.e., one half of it). The sensor includes three parts: a rigid base, block 1, and block 2. Block 1 is a tube that is made of an elastic material and has Young's modulus of E_1. Block 2 is a cylinder that is made of another elastic material and has Young's modulus of E_2. The rigid base is a combination of two cylinders of different diameters and has a much larger Young's modulus than those of blocks 1 and 2. One PVDF film (polyvinylidene fluoride), which is indicated as PVDF1, is attached to block 1 and located between block 1 and the rigid base. PVDF1 generates a voltage of V_1, which is proportional to the stress applied to the end face of block 1.[25–30] Another PVDF film (PVDF2) is attached to block 2 and located between block 2 and the rigid base. PVDF2, in turn, produces a voltage of V_2 which is proportional to the stress applied to the end face of block 2. Although the end faces of blocks 1 and 2 touch the surface of the tissue, they receive different strains and stresses. The Young's modulus of the touched tissue is obtained by comparing the outputs of PVDF1 and PVDF2.

On the basis of the computer-generated model, a number of sensors were fabricated. A photograph of one of the sensors is shown in Fig. 2. In our work, E_1, E_2, and the modulus of elasticity for the rigid base were 1×10^2, 1×10^5, and 1×10^7 Pa and Poisson's ratios were 0.48, 0.40, and 0.38, respectively. Here, two 110-μm-thick metalized and uniaxially poled PVDF films (Good Fellow Company, USA) were placed between the rigid base and the blocks, that is, beneath blocks 1 and 2. Both of the films were attached using double-sided adhesive tape. A 2 mm by 1 mm channel groove was cut on the bottom of block 1 to isolate the output PVDF film channel that was under block 2 and intersected with block 1.

2.2 *Experimental setup*

A rectangular block was made of silicon rubber in which two spherical objects with the same modulus of elasticity (i.e., $E_{\text{object}} = 1\times10^5$ Pa) were embedded. Poisson's ratio (ν) for the objects was 0.45. E_{matrix} was 1×10^3 Pa with $\nu = 0.40$. In the experimental runs, there were no noticeable interferences or crosstalks.[31–35] In this configuration, the charge coming out via the PVDF film under the block 2 cylinder represented the force applied to

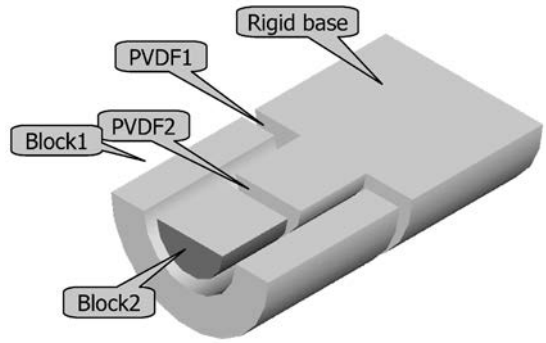

Fig. 1. Schematic of sensor.

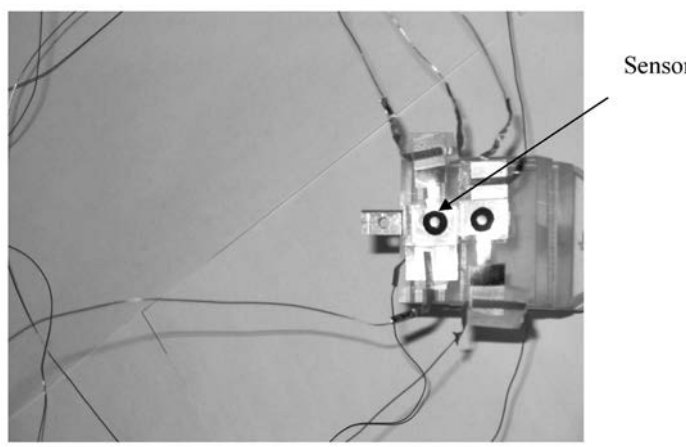

Fig. 2. Photograph of designed sensor.

it. Correspondingly, the charge coming out via the PVDF film below block 1 represented the force applied to this piezoelectric film. The magnitude of the applied force was determined by a force transducer (Kistler, Type 9712B50). The charges generated by both PVDF films were amplified by a charge amplifier (D. J. Birchal model 04) and the output was measured using an oscilloscope (Agilent 54624A). One channel of the oscilloscope was used to measure the output of PVDF1 and another channel for the output of PVDF2. A dynamic load was applied to the block made of silicon rubber with the following dimensions: length = 10 cm, breadth = 8 cm and depth = 6 cm. Peak-to-peak voltage and frequency from the channels were captured by data acquisition using the interface system.[36]

2.3 *Mathematical formulation*

The main purpose of the system is to measure the stiffness of embedded objects. The operation of the tactile sensor is based on the ability to measure relative deformation between adjacent parts of the sensor. The method adopted here was to apply force to the test object (i.e., the rubberlike block) such that a part of the object was supported by the block 2 and the rest by block 1 in the sensor. In the designed system, A_2 and A_1 are the cross-sectional areas of block 2 and block 1 cylinders, respectively, and the ratio of A_2/A_1 is 3.7.

Owing to the physical structure of the system under study, it can be shown that a force acting on the elastic solid only affects a part of the solid, not the entire solid. This finding is different from the convention of Hooke's law. As a result, we decided to use a more complex and more accurate theory of elastodynamics in our calculations. Figure 3 shows what happens to the sensor and tissue as the sensor is pressed against the tissue surface. The left side of the figure is the status before applying force, whereas the right side is the status after applying force.

We propose an analytical method (Fig. 4), by which an estimate of the stiffness of embedded objects can be obtained (i.e., E_{object} or E_{tumor}). Additionally, we derive a

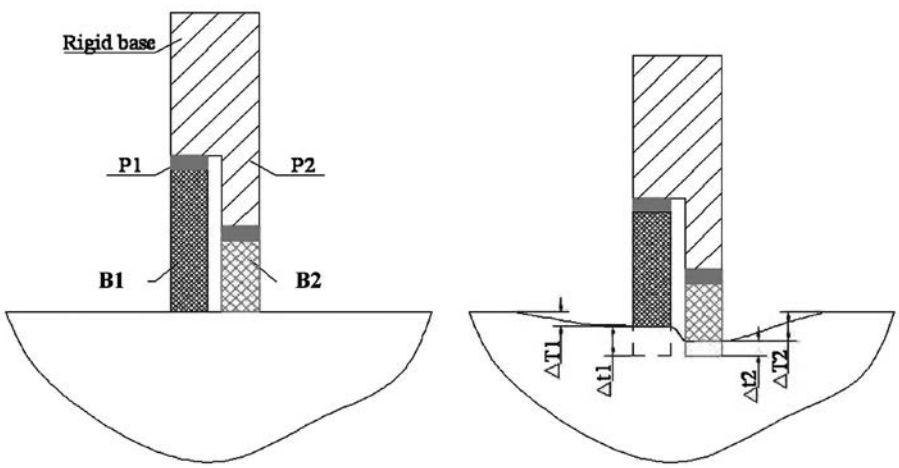

Fig. 3. Deformation of sensor-tissue assembly when pressing probe against tissue.

relationship that can provide information on the depth or location of a tumor or object. In this figure, the outer rectangle is tissue, while the inner circle is a simulated tumor. A normal stress of σ is applied to a circular surface whose diameter is 2*a*. Here, Poisson's ratio of the tissue is shown by *v*. According to the solution of Boussinesq's problem,[37,38]

$$\sigma_1 = \frac{3\sigma a^2}{2d^2}. \tag{1}$$

The displacement of point *A* without considering the effect of the tumor is

$$DIS_{\mathrm{A}} = \frac{2(1-v^2)\sigma a}{E_{\mathrm{matrix}}}. \tag{2}$$

Because the tumor is much smaller than the tissue, it can be treated mathematically as follows:

$$\varepsilon = \frac{\sigma_1}{E_{\mathrm{object}}} \Rightarrow DIS_B = \frac{\sigma_1 D}{E_{\mathrm{object}}} = \frac{3\sigma a^2 D}{2d^2 E_{\mathrm{object}}}, \qquad \sigma_1 = \sigma_2. \tag{3}$$

The displacement of point *C* is

$$DIS_{\mathrm{C}} = \frac{3(1-v^2)\sigma a^2 D}{2E_{\mathrm{matrix}} d^2}. \tag{4}$$

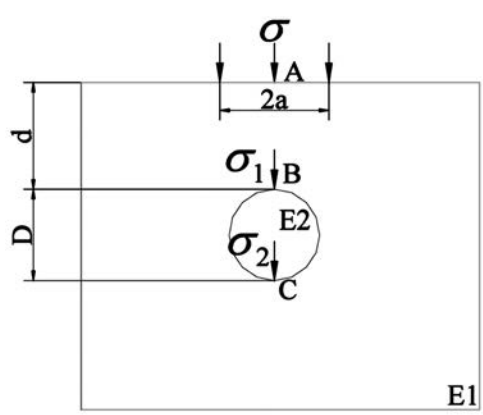

Fig. 4. Physical model used in deriving stiffness of embedded object.

By assuming that the general or equivalent Young's modulus for the whole tissue plus the objects is equal to E_{eq} , we can show that the general displacement of point *A* is

$$DIS = \frac{2(1-v^2)\sigma a}{E_{eq}}. \tag{5}$$

Using a compatibility equation for the displacements, we have

$$DIS = DIS_A + DIS_B + DIS_C. \tag{6}$$

By substituting for the displacements in the above equation, the following relationship is obtained:

$$\frac{2(1-v^2)\sigma a}{E_{eq}} = \frac{2(1-v^2)\sigma a}{E_{matrix}} + \frac{3\sigma a^2 D}{2d^2 E_{object}} + \frac{3(1-v^2)\sigma a^2 D}{2E_{matrix} d^2}. \tag{7}$$

By rearranging the above relationship, we arrive at the following equation for E_{eq}:

$$E_{eq} = \frac{4E_{matrix}E_{object}(1-v^2)d^2}{E_{object}(1-v)^2(4d^2+3aD)+3aDE_{matrix}}. \tag{8}$$

The parameter "*a*" which is used in the above equation can be readily obtained from the characteristics of our designed sensor. Hence, E_{eq} will be calculated using Young's modulus of the parent tissue (E_{matrix}), Young's modulus of the tumor (E_{object}), the depth of the tumor (d), and the diameter of the tumor (D). Consequently, the above equation contains information on an important physical characteristic of the embedded object, that is, the diameter of the object.

By modifying eq. (8), we can derive an operational equation for the computation of E_{object} (see Fig. 5). The following parameters are defined in the proposed model:

(1) Tissue 1 has a thickness of T_1, Young's modulus of E_1, and Poisson's ratio of v_1.
(2) The tumor has a thickness of T_2, Young's modulus of E_2, and Poisson's ratio of v_2.
(3) Tissue 2 has a thickness of T_3, Young's modulus of E_1, and Poisson's ratio of v_1.
(4) The radius for the circular region of the applied force is equal to a.

According to the elastodynamics theory, we have

$$\Delta T_1 = \frac{2(1-v_1^2)\sigma a}{E_1};\ \Delta T_2 = \frac{2(1-v_2^2)\sigma a}{E_1};\ \Delta T_3 = \frac{2(1-v_1^2)\sigma a}{E_1}. \tag{9}$$

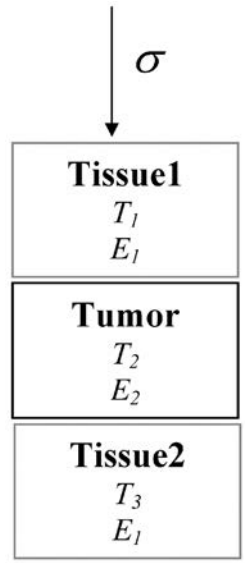

Fig. 5. Determining relationship between E_{eq} and other moduli.

Generally, $v_1 = v_2$; therefore,

$$E_{eq} = \frac{2(1-v_1^2)\sigma a}{\Delta T} = \frac{2(1-v_1^2)\sigma a}{\Delta T_1 + \Delta T_2 + \Delta T_3}. \tag{10}$$

Thus,

$$E_{eq} = \frac{1}{\frac{1}{E_1} + \frac{1}{E_2} + \frac{1}{E_3}}. \tag{11}$$

We can use eq. (11) to find Young's modulus of the embedded object ($E_2 = E_{object}$). Following this, and by obtaining E_{eq}, E_1 (or E_{matrix}) and E_2 (or E_{object}), the diameter of the tumor can also be easily determined using eq. (8).

2.4 *Finite element modeling*

The human skin and its sublayers are all soft tissues and their softness is approximately constant over a certain range in the same organ. Following this, in our model, we consider the system to have a constant stiffness over the studied region. As such, we have selected rubber to be the simulation parent material for a human organ. Similarly to the experimental work, a block of a rubberlike material is made and modeled using both the analytical approach and a finite element analysis method. The dimensions of the simulated block are length = 10 cm, breadth = 8 cm, and depth = 6 cm. Figure 6 shows a drawing of the block

together with the sensing probe located on top of the block. Inside this block, we embedded two spherical objects (with 50 and 80 mm in diameters) with the appropriate mechanical properties to simulate cancer tumors.

The purpose of the simulation is to model the phenomenon of tissue deformation caused by an applied force and to predict the stiffness of embedded objects. The entire process of modeling was practically achieved by trial-and-error. Under applied loads of 1, 5 and 10 N for the specified locations on the surface of the block, we assumed different E's for the embedded object and then performed the modeling (i.e., the first iteration). Poisson's ratio for the objects was assumed to be constant and equal to 0.45. The deformations obtained by numerical analysis were then compared with experimental values. This process continued until the experimental and the numerical data matched. As such, E_{object} for the last iteration was taken as the simulation result. Owing to the complexity of the system, which is highly nonlinear with complex contact features between various surfaces, a commercial finite element analysis software package (ANSYS, version 8.0) was employed. We used RTV6166 2 part silicone rubber. For the probe assembly, various types of element were adopted for different parts of the structure. In the case of the rigid base, the SOLID 45 element was used, whereas for the PVDF films, we used the SOLID 95

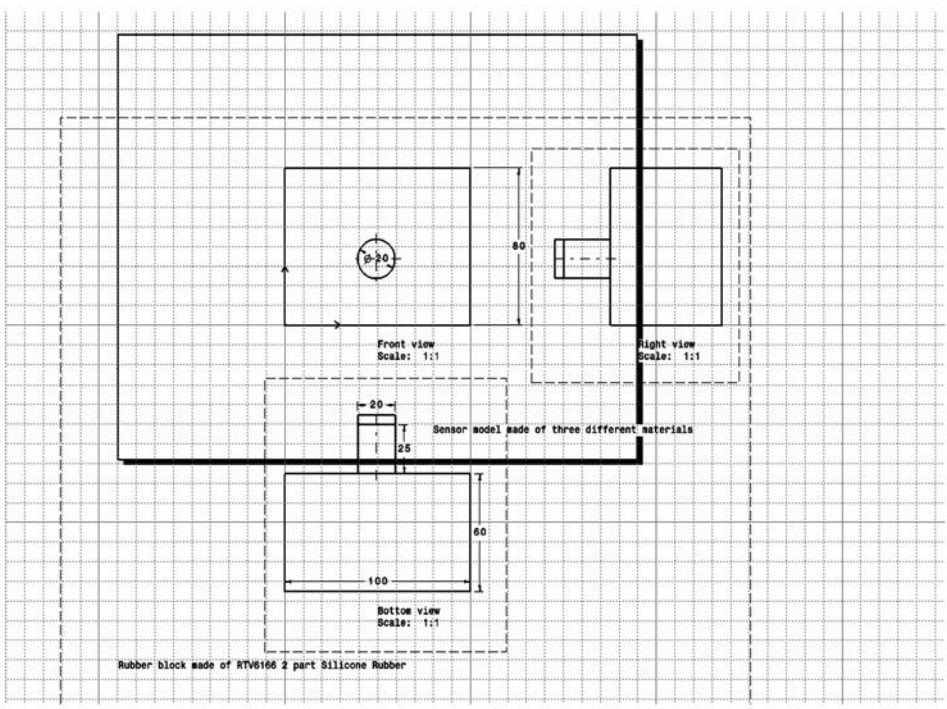

Fig. 6. Drawing of block used in numerical simulations (dimensions in mm).

element was used. The software package generated a model of the problem on the basis of the input data. This model is shown in Fig. 7.

The stresses that developed in the system (because of the applied forces) can be correlated with output charge using the following formulation. When a force is applied to the PVDF sensor, the output charge from each PVDF sensing element is, in effect, the sum of the piezoelectric coefficients d_{31}, d_{32} and d_{33} in the drawn, transverse, and thickness directions, respectively, multiplied by the magnitude of the applied force. In mathematical form, we have[8]

$$F = \frac{Q}{\psi_1 d_{31} + \psi_2 d_{32} + d_{33}}, \tag{12}$$

where Q is the output charge, F is the applied force on the sensing element, and ψ_1 and ψ_2 are constants proportional to the electrode area of the sensing elements. Table 1 shows the summary of the piezoelectric coefficients of the PVDF film, obtained from the manufacturer's technical specifications.

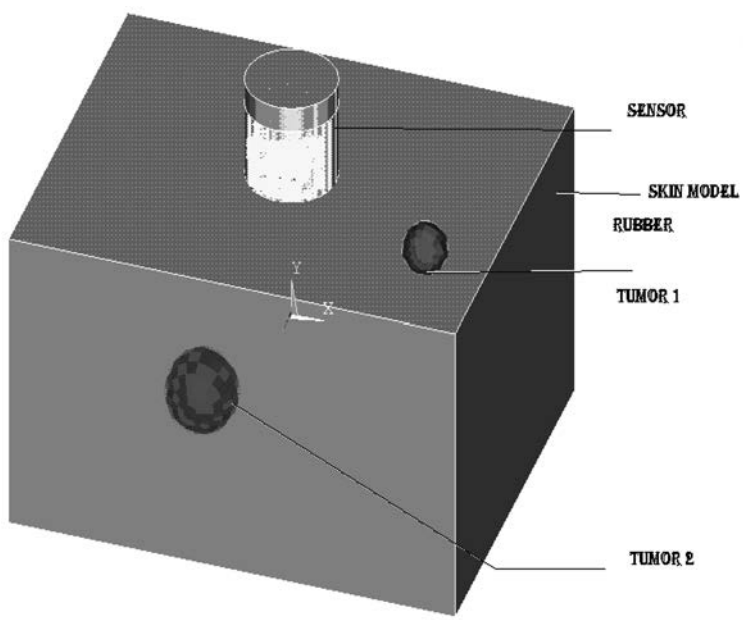

Fig. 7. Model of block-probe assembly generated in ANSYS.

3. Results and Discussion

We selected four different positions for the application of various loads of 1, 5 and 10 N. The details of these positions are given in Table 2. Figure 8 represents the ANSYS-generated models for the different positions, whereas Fig. 9 shows a typical simulation output obtained when the probe was applied at position 4.

For comparison, we chose the y-direction component of the stress on the surface of the sensor. In this plane, there are two kinds of material; one is the inner solid cylinder (i.e., block 2) and the other is the outer hollow cylinder (i.e., block 1). These two parts are made of different materials that have different properties. Therefore, their stresses are not the same. We used stress 1 as the stress on the inner cylinder and stress 2 as the stress on the outer hollow cylinder. Both the analytical and numerical methods (using ANSYS) were used and nearly similar results were obtained for these stresses. Table 3 shows a summary of the results obtained by the numerical approach.

The data we obtained from each position and each applied load indicate that because the inner solid cylinder is harder than the outer hollow cylinder, stress 1 becomes larger than stress 2. This phenomenon can easily be proven for all four positions. After comparing the results obtained from different positions, it can be noted that stress 1 and stress 2 are both affected by the position. When the sensor is applied to the top of each tumor, we obtain larger stress 1 and stress 2, because the tumor is harder than the surrounding tissue. Additionally, when the sensor is applied to top of tumor 1, the stress values are larger than those when the sensor is applied to tumor 2. This is because tumor 1 is larger than tumor 2 (i.e., 60% larger).

It should be pointed out that in the design of the sensor, there is a gap of 0.1 mm between blocks 1 and 2. The reason for this gap was to eliminate friction between the two concentric cylinders; hence, allowing the sensor to operate more smoothly. Gaps larger than the prescribed value made the device less robust. Therefore, in theory, there should be no contact between these two structures. Although the emphasis of this work was at a force of 1 N, in some of the experimental runs when forces of about 2 N were exerted, some distortion was observed in the sensor. This could mean that shear force within the system cannot be neglected in all runs. Eliminating this possible shear force is not difficult. It can be eliminated by increasing the gap between blocks 1 and 2. Although it is difficult to account for the various possible errors in the measurements (such as external vibrations originating from the environment), it was estimated that the contribution of these errors was about 5%.

Table 1
Piezoelectric coefficients of PVDF film.

Piezoelectric coefficient			
d-form (pC/N)		*g*-form (Vm/N)	
d_{31}	20	g_{31}	0.15
d_{32}	2	g_{32}	0.015
d_{33}	–20	g_{33}	–0.15

Table 2
Different positions for application of various loads.

Position No.	Location
1	Between tumors 1 and 2
2	On top of tumor 2
3	On top of tumor 1
4	Far away from tumors 1 and 2

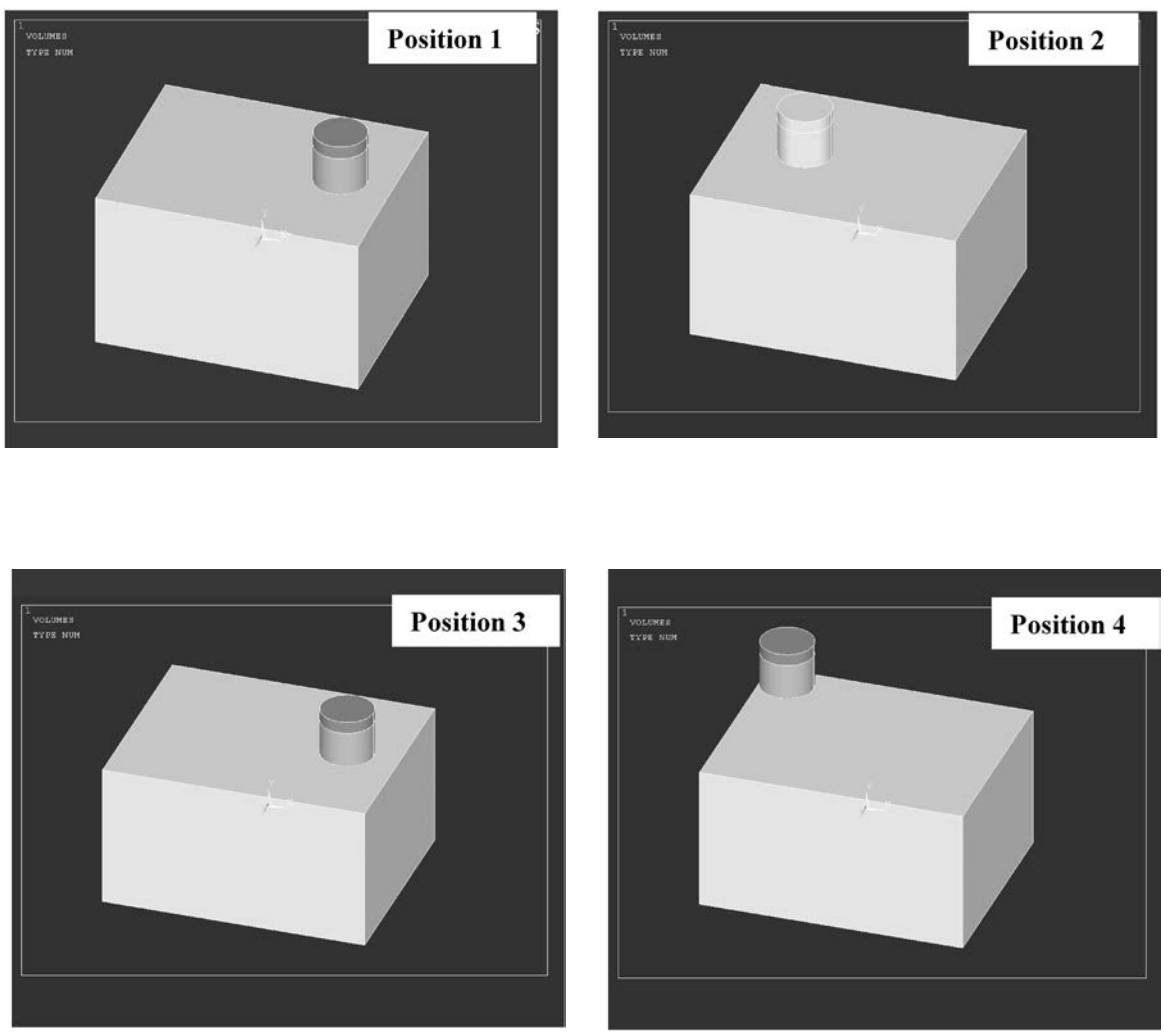

Fig. 8. Models of various sensing probe positions (positions 1 to 4).

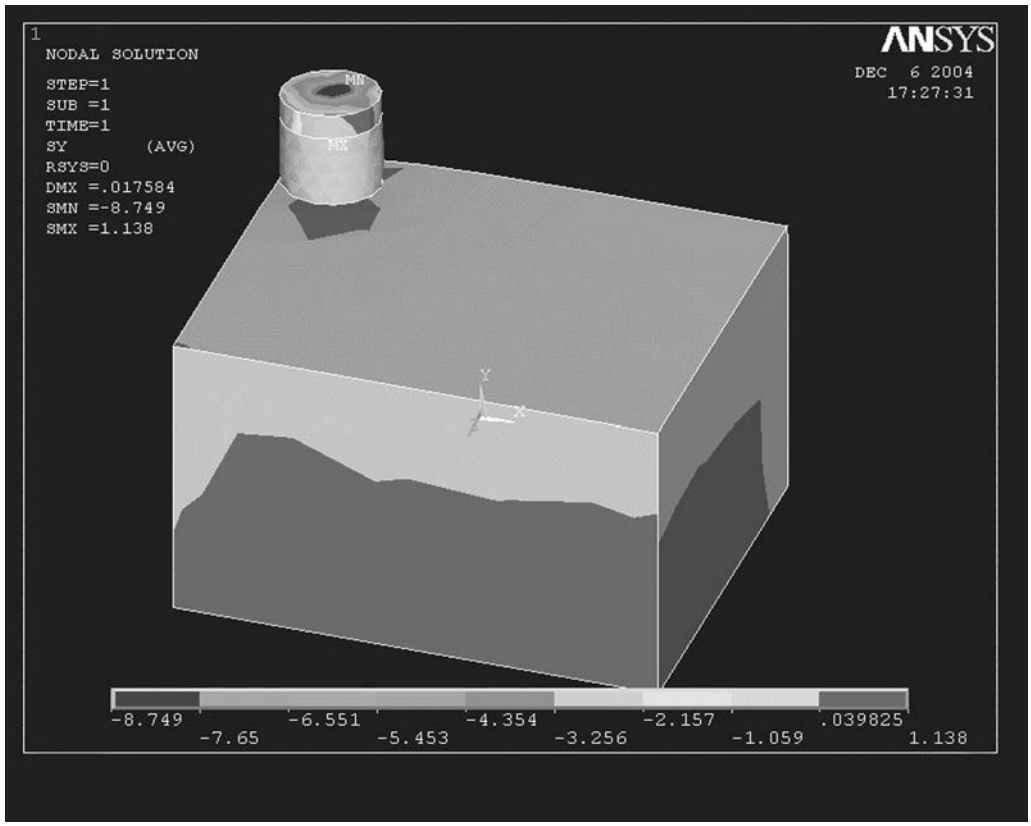

Fig. 9. Deformation of sensor when probe is applied at position 4.

Table 3
Sensor stresses for various probe positions.

Position	Stress		Stress 1/Stress 2
Position 1	Stress 1	Stress 2	
1 N	–2.371	–1.571	1.50923
5 N	–11.859	–7.857	1.509355
10 N	–23.718	–15.715	1.509259
Position 2			
1 N	–2.728	–1.791	1.523171
5 N	–13.639	–8.956	1.52289
10 N	–27.277	–17.912	1.522834
Position 3			
1 N	–1.61	–0.61794	2.60543
5 N	–8.05	–3.09	2.605178
10 N	–16.1	–6.179	2.6056
Position 4			
1 N	–1.059	0.039825	26.59134
5 N	–5.294	0.199124	26.58645
10 N	–10.587	0.398248	26.58395

The error in the output of the finite element method (i.e., the stiffness of the embedded object) was about 20%, when compared with the actual reported value. This is very close to the stiffness computed using the analytical approach we developed. An average discrepancy of about 7% was observed between the finite element and analytical methods.

A major advantage of the designed probe is that it can be easily miniaturized and micromachined. Therefore, it could be mass produced at a low cost and even become disposable. This is of great importance when dealing with biological tissues. By making the head of the probe disposable, we would be reducing the possibility of cross-contamination.

The results of this research have important applications in the detection of tumors embedded in a biological tissue (for example, tumors in the human breast). The experimental studies and theoretical modeling of cases in which objects with different geometries and compliances are embedded in the block are currently underway in our laboratory. Determining the exact location of tumors is another research area that needs to be explored in more detail.

Acknowledgments

We would like to express our gratitude to Dr. H. Scarth (the Chief Surgeon at Saint John Regional Hospital, Saint John, Canada) and Professor M. Anvari (the Director of the Centre for Minimal Access Surgery at McMaster University, Hamilton, Canada) for valuable comments and suggestions on the clinical aspects of this research. The authors also thank the Institute for Robotics and Intelligent Systems (IRIS) and Natural Sciences and Engineering Research Council (NSERC) of Canada for providing financial support.

References

1 C. M. Kaelin and F. Coltrera: Living Through Breast Cancer (McGraw Hill Co., 2005).
2 A. E. Kerdok, S. M. Cotin, M. P. Ottensmeyer, A. M. Galea, R. D. Howe and S. L. Dawson: Medical Image Analysis **7** (2003) 283.
3 J. Dargahi and S. Najarian: Canadian Journal of Electrical and Computer Engineering **28** (2003) 155.
4 J. Dargahi and S. Najarian: Sensor Review **24** (2004) 74.
5 J. Dargahi and S. Najarian: Bio-Medical Materials and Engineering **14** (2004) 151.
6 J. Dargahi and S. Najarian: Sensors and Materials **16** (2004) 25.
7 I. Brouwer, J. Ustin, L. Bentley, A. Sherman, N. Dhruv, and F. Tendick: Studies in Health Technology Informatics - Medicine Meets Virtual Reality (ISO Press, Amsterdam, 2001).
8 J. Dargahi and S. Najarian: Sensor Review **24** (2004) 284.
9 P. Dario: Sens. Actuators, A **26 (**1991) 251.
10 J. Dargahi and S. Najarian: International Journal of Medical Robotics and Computer Assisted Surgery **1** (2004) 23.
11 B. Hannaford, J. Trujillo, M. Sinanan, M. Moreyra, J. Rosen, J. Brown, R. Leuschke and M. MacFarlane: Medicine Meets Virtual Reality (ISO Press, Amsterdam, 1998).
12 J. Dargahi and S. Najarian: Industrial Robot **32** (2005) 268.
13 J. Dargahi, S. Najarian and K. Najarian: Canadian Journal of Electrical and Computer Engineering **30** (2005) 225.
14 J. Dargahi, S. Najarian and X. Z. Zheng: Sensors and Materials **17** (2005) 7.

15 A. Bicchi, G. Canepa, D. De Rossi, P. Iacconi and E. P. Scilingo: International Conference on Robotics and Automation 1996 (IEEE, Minneapolis, 1996) p. 884.
16 R. D. Howe, W. J. Peine, D. A. Kontarinis and J. S. Son: IEEE Engineering in Medicine and Biology Magazine **14** (1994) 318.
17 J. Dargahi, S. Payandeh and M. Parameswaran: International Conference on Robotics and Automation 1999 (IEEE, Detroit, 1999) p. 299.
18 J. Dargahi, M. Parameswaran and S. Payandeh: Journal of Microelectromechanical Systems **9** (2000) 329.
19 P. Dario, M. C. Carrozza, L. Lencioni, B. Magnani and S. D'Attanasio: International Conference on Robotics and Automation 1997 (IEEE, Albuquerque, 1997) p. 1567.
20 J. Dargahi: Journal of Mechanical Design **124** (2002) 576.
21 H. Singh, J. Dargahi and R. Sedaghati: 2nd International Conference on Sensors 2003 (IEEE, Toronto, 2003).
22 N. P. Rao, J. Dargahi, M. Kahrizi and S. Prasad: Canadian Conference on Electrical and Computer Engineering 2003 (CCECE, Montreal, 2003).
23 H. Fischer, B. Neisius and R. Trapp: Interactive Technology and a New Paradigm for Health Care (IOS Press, Amsterdam, 1995).
24 J. Dargahi: CSME International Conference 2001 (CSME, Montreal, 2001) p. 21.
25 J. Dargahi and S. Payandeh: International Conference on Sensor Fusion: Architectures Algorithms and Applications 1998 (SPIE, Orlando, 1998) p. 122.
26 J. Dargahi: Sens. Actuators, A **80** (2000) 23.
27 H. H. Melzer, M. O. Schurr, W. Kunert, G. Buess, U. Voges and J. U. Meyer: Endoscopic Surgery and Allied Technologies **1** (1993) 165.
28 J. Dargahi: Sens. Actuators, A **71 (**1998) 89.
29 M. H. Lee and H. R. Nicholls: Mechatronics **9** (1999) 1.
30 Y. Bar-Cohen, C. Mavroidis, M. Bouzit, B. Dolgin, D. Harm, G. Kopchok and R. White: Proc. Int. Conf. for Smart Systems and Robotics for Medicine and Space Applications 2000, (IEEE, Houston, 2000).
31 E. Crago, J. Nakai, and H. J. Chizeck: IEEE Transactions on Biomedical Engineering **38** (1991) 17.
32 B. Gray and R. S. Fearing: International Conference on Robotics and Automation 1996 (IEEE, Minneapolis, 1996) p. 1.
33 J. Dargahi, A. Eastwood and I. J. Kemp: International Conference on Sensor Fusion: Architectures Algorithms and Applications 1997 (SPIE, Orlando, 1997) p. 20.
34 J. Dargahi, The Application of Polyvinylidene Fluoride as a Robotic Tactile Sensor, Ph.D. dissertation (Glasgow Caledonian University, Glasgow, 1993).
35 R. S. Fearing, G. Moy and E. Tan: International Conference on Robotics and Automation 1997 (IEEE, Albuquerque, 1997) p. 3093.
36 A. Fisch, C. Mavroidis, J. Melli-Huber and Y. Bar-Cohen: Inspired Intelligent Robots (SPIE Press, Bellingham, 2003).
37 C. J. C. Cordova: Elastodynamics With Hysteretic Damping (Delft University Press, 2004).
38 A. C. Eringen and E.S. Suhubi: Elastodynamics (Academic Press, New York, 1975).